Naval Research Laboratory
Washington, DC 20375-5320

NRL/5610/MR—2023/3

Photon Pair Generation by Four Wave Mixing in an Atomic Ensemble

SUNIL UPADHYAY

ADAM BLACK

Optical Physics Branch
Optical Sciences Division

December 18, 2023

REPORT DOCUMENTATION PAGE

Form Approved
OMB No. 0704-0188

1. REPORT DATE *(DD-MM-YYYY)*	**2. REPORT TYPE**	**3. DATES COVERED** *(From - To)*
18-12-2023	NRL Memorandum Report	

4. TITLE AND SUBTITLE

Photon Pair Generation by Four Wave Mixing in an Atomic Ensemble

5a. CONTRACT NUMBER

5b. GRANT NUMBER

5c. PROGRAM ELEMENT NUMBER

6. AUTHOR(S)

Sunil Upadhyay and Adam Black

5d. PROJECT NUMBER

5e. TASK NUMBER

5f. WORK UNIT NUMBER
1V12

7. PERFORMING ORGANIZATION NAME(S) AND ADDRESS(ES)

Naval Research Laboratory
4555 Overlook Avenue, SW
Washington, DC 20375-5320

8. PERFORMING ORGANIZATION REPORT NUMBER

NRL/5610/MR--2023/3

9. SPONSORING / MONITORING AGENCY NAME(S) AND ADDRESS(ES)

Office of Naval Research
One Liberty Center
875 N. Randolph Street, Suite 1425
Arlington, VA 22203-1995

10. SPONSOR / MONITOR'S ACRONYM(S)

ONR

11. SPONSOR / MONITOR'S REPORT NUMBER(S)

12. DISTRIBUTION / AVAILABILITY STATEMENT

DISTRIBUTION STATEMENT A: Approved for public release; distribution is unlimited.

13. SUPPLEMENTARY NOTES

14. ABSTRACT

Pump laser beam configurations for the generation of nonclassically correlated photon pairs in laser-cooled rubidium ensembles were investigated experimentally. Departing from past near-resonance single-pump configurations, we investigated both off-resonance and multi-frequency pump configurations that may be capable of generating hyperentangled photon pairs that are relevant for quantum communication applications. We characterized the falloff in violation of the Cauchy-Schwartz inequality that takes place as the pump is detuned from resonance and as additional frequencies are added.

15. SUBJECT TERMS

16. SECURITY CLASSIFICATION OF:			**17. LIMITATION OF ABSTRACT**	**18. NUMBER OF PAGES**	**19a. NAME OF RESPONSIBLE PERSON**
					Adam Black
a. REPORT	**b. ABSTRACT**	**c. THIS PAGE**	U	25	**19b. TELEPHONE NUMBER** *(include area code)*
U	U	U			(202) 404-2573

This page intentionally left blank.

EXECUTIVE SUMMARY

The research described herein is an investigation of schemes for the generation of nonclassically correlated or entangled photon pairs in a laser-cooled rubidium ensemble. In particular, we wish to develop schemes that may lead to the efficient production of photons that are entangled in multiple degrees of freedom, sometimes referred to as "hyperentangled" photons. Hyperentangled photons have been proposed as a resource for quantum secure direct communication and superdense coding, efficient Bell-state measurement for quantum teleportation and quantum repeater demonstrations, and even optical sensing with improved resolution.

We focus on simple pump laser schemes that make use of a single, retroreflected laser beam and perform experiments to determine the viability of variations on a simple, read-on-resonance scheme. We vary the pump detuning to increase the probability of the simultaneous operation of multiple four-wave-mixing processes. We also add phase-modulation sidebands to the pump laser to drive multiple near-resonance processes. We additionally alter the aspect ratio of the pump, effectively changing the Fresnel number of the participating atomic sample. We also perform four-wave-mixing experiments with the cold-atom ensemble optically pumped to a single magnetic sublevel.

As part of this work, we developed a cold-atom apparatus that attempts to achieve multiple goals simultaneously: high optical depth (the threshold criterion for photon pair generation), sub-Doppler cooling, efficient optical pumping, and high repetition rate.

This page intentionally left blank

PHOTON PAIR GENERATION BY FOUR WAVE MIXING IN AN ATOMIC ENSEMBLE

1. INTRODUCTION

Laser-cooled atoms are an important tool for the study of fundamental light-matter interactions and for applications in quantum optics and quantum information. The ability to control interactions between laser light and atoms is vital in frontier research areas such as quantum computation and quantum communication [1, 2]. For quantum communication in particular, two key requirements must be fulfilled: photons that encode and transmit information, and remote quantum memories that can receive, store, and retransmit the photon state. The generation of quantum states of light that are compatible with storage in a quantum memory is thus an important goal. This can be achieved by generating narrowband photons in an atomic ensemble that is also capable of operation as a quantum memory.

Photon pairs entangled in more than one degree of freedom, often called hyperentangled photons, are desirable since they can carry more information per photon [3]. They can also employ one degree of freedom of entanglement as an ancilla to enable complex operations. Generation of hyperentangled photon pairs has been demonstrated in a variety of systems: non-linear crystals [3], quantum dots [4], and atomic ensembles [5, 6]. Solid-state systems such as β-barium borate [3] and periodically poled lithium niobate [7] can be used to generate hyperentangled photon pairs at a high rate, but the resulting pairs have optical bandwidths on the order of 1 nm. The large bandwidth prevents an efficient interface with long-duration quantum memories such as cold atomic ensembles, whose optical linewidths are on the order of 6 MHz. On the other hand, despite narrow-linewidth photon pair generation, cold-atom experiments exhibit a relatively low rate of photon emission and require an optically dense sample of atoms [8, 9].

Key results in hyperentangled photon pair generation in cold atoms were obtained by Yan et al. [10] and Zhao et al. [6]. The underlying physics that governs the non-classical correlations between the photons in a pair was studied earlier by Lukin et al. [11, 12] and are based on enhancement of nonlinear optical processes using electromagnetically induced transparency (EIT) studied by Harris et al. [13]. Further experimental and theoretical details can be found in the work of Balic et al. [9] and Kolchin et al. [14] and references therein.

Relevant prior works [6, 10] in atomic ensembles have exploited EIT-based Λ-level schemes with an off-resonant write beam and a near-resonant read beam. In contrast, our primary proposed implementation uses a single pump field that is detuned by roughly half the ground state hyperfine splitting of ^{87}Rb for both the read and the write process. For atoms optically pumped to the central magnetic sublevel in the rubidium hyperfine ground state, the electric dipole selection rules may allow four different four-wave-mixing processes to take place simultaneously. The intended outcome of this scheme is the interference of these four processes to produce photons entangled in both polarization and frequency, with the emitted frequencies differing by the ^{87}Rb ground-state hyperfine splitting. In this work we have performed experiments to determine whether the process of quantum correlated photon generation persists with this alteration in the pumping configuration compared with prior work. We present the details of the level scheme, experimental setup, and measurements

Manuscript approved December 15, 2023.

of quantum correlated photon production. This scheme is called the Raman scheme hereafter. Additionally, we have carried out experiments using a multilevel EIT-based scheme not explored hitherto in literature. This scheme is called the EIT scheme hereafter. We present experimental findings in this report.

2. PROPOSED METHODS

2.1 Raman scheme

Consider the level diagram of figure 2 and the geometric configuration of cold atoms and write/read beam in figure 3. All the relevant energy levels of ^{87}Rb are shown in figure 1. We start with all the atoms initialized by optical pumping in the $|F = 1, m_F = 0\rangle$ state. Upon optical excitation by a π-polarized "write" beam red-detuned by $\Delta_{HF}/2$ from $P_{3/2}$, an atom in $|F = 1, m_F = 0\rangle$ can Rayleigh scatter into states $|F = 1, m_F = \pm 1\rangle$ or Raman scatter into states $|F = 2, m_F = \pm 1\rangle$ with some probabilities. This atom can undergo another optical excitation when illuminated by a counter propagating "read" beam (provided by a retroreflection of the write beam), followed by another set of Rayleigh scattering or Raman scattering back into the original state with some probability. There are thus four different Raman scattering paths due to the write-read process where the atoms start and end in the same initial state $|F = 1, m_F = 0\rangle$ as required by the four-wave-mixing process. These pathways are listed in table 1.

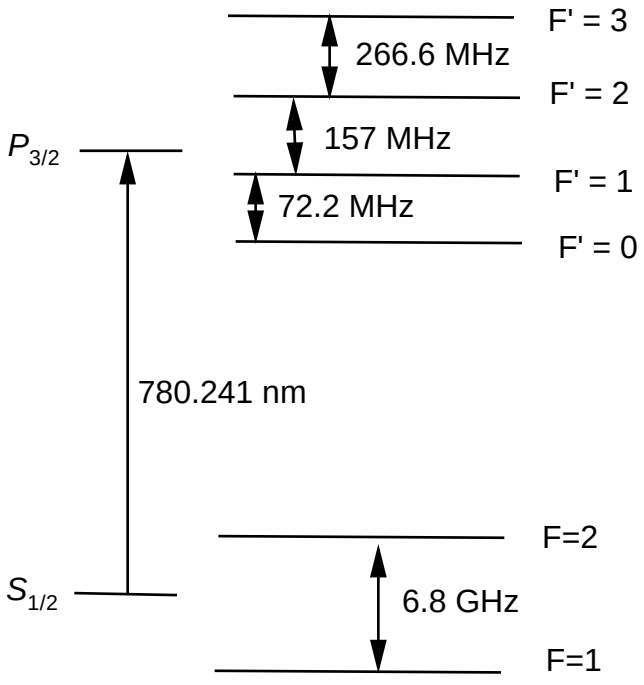

Fig. 1—^{87}Rb D_2 transition hyperfine structure.

The probability amplitudes for these four paths can interfere, leading to correlations between the spontaneously emitted photon pairs (shown by wavy dashed lines in figure 2). One can understand this correlation in a manner similar to polarization correlations between photons in Aspect's landmark experiment described in reference [15]. Due to conservation of energy and angular momentum in the process, the

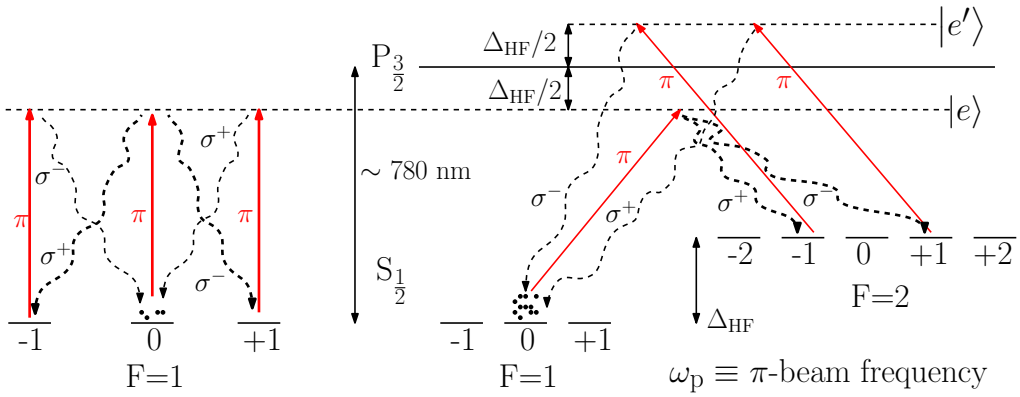

Fig. 2—Schematic of level scheme for hyperentangled photon pair production using ^{87}Rb D_2-line. No hyperfine states are shown for the excited state. $|e\rangle$ and $|e'\rangle$ are two "virtual" states detuned to the red and the blue side of the optical transition by $\Delta_{HF}/2$. Solid straight lines indicate absorption and dashed wavy lines indicate spontaneous emission.

Path #	Paths
1	$\|F=1, m_F=0\rangle \rightarrow \|e\rangle \rightarrow \|F=1, m_F=-1\rangle \rightarrow \|e\rangle \rightarrow \|F=1, m_F=0\rangle$
2	$\|F=1, m_F=0\rangle \rightarrow \|e\rangle \rightarrow \|F=1, m_F=+1\rangle \rightarrow \|e\rangle \rightarrow \|F=1, m_F=0\rangle$
3	$\|F=1, m_F=0\rangle \rightarrow \|e\rangle \rightarrow \|F=2, m_F=-1\rangle \rightarrow \|e'\rangle \rightarrow \|F=1, m_F=0\rangle$
4	$\|F=1, m_F=0\rangle \rightarrow \|e\rangle \rightarrow \|F=2, m_F=+1\rangle \rightarrow \|e'\rangle \rightarrow \|F=1, m_F=0\rangle$

Table 1—Four allowed four-photon absorption and emission paths indicated in figure 2 and discussed in the text.

entangled state of the photon pairs emitted is of the form:

$$\Psi \propto \left(\alpha \left|\sigma^+\right\rangle_1 \left|\sigma^-\right\rangle_2 + \beta \left|\sigma^-\right\rangle_1 \left|\sigma^+\right\rangle_2\right) \bigotimes \left(\gamma \left|\omega_p\right\rangle_1 \left|\omega_p\right\rangle_2 + \chi \left|\omega_p - \Delta_{HF}\right\rangle_1 \left|\omega_p + \Delta_{HF}\right\rangle_2\right) \quad (1)$$

where α, β, γ, and χ are complex constants. Δ_{HF} is the hyperfine splitting between the ground F=1 and F=2 levels as shown in figure 2. ω_P is the frequency of the linearly polarized write/read laser beam. The linearly polarized laser beam drives π-transitions with respect to the quantization axis defined by a small bias-field indicated in figure 3. σ^+ and σ^- refer to left-hand circularly polarized and right-hand circularly polarized photons, respectively, emitted via spontaneous decay as shown in figure 2.

Additionally, conservation of linear momentum (part of the phase matching condition) leads to entanglement in the wave vector degree of freedom. The choice of quantization direction indicated in figure 3 along with linear momentum conservation dictate that the probability of σ^+/σ^- photon pair emission is maximum in the direction perpendicular to the incident write/read beams. Due to the orientation of the electric field vector of the write/read beam, the undesired background of Rayleigh-scattered π-polarized light is also minimized along this direction.

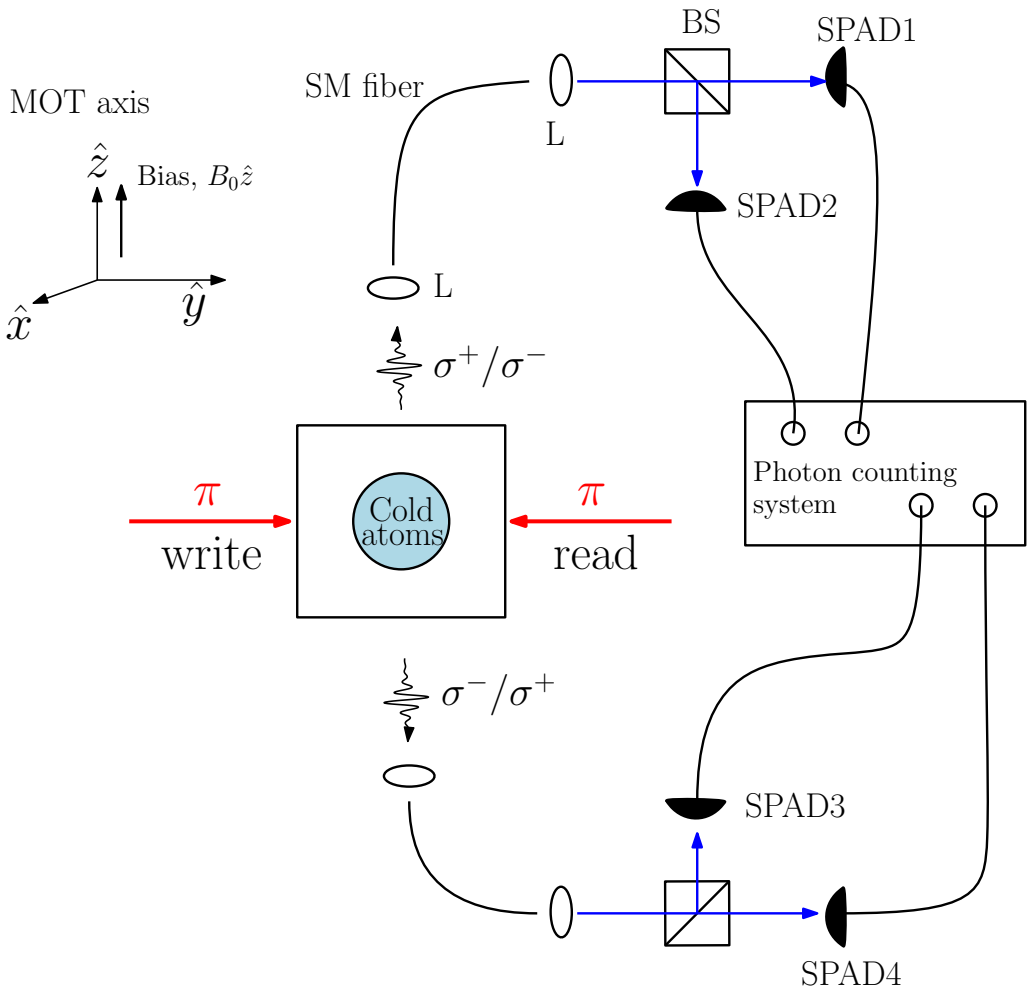

Fig. 3—Schematic of a cold atom setup for entangled photon pair generation and characterization. The quantization direction is defined by a small bias field along the $\hat{z}$ direction. A π-polarized write laser beam is retroreflected and serves as the read beam. L, SM fiber, BS, and SPAD refer to lens, single-mode fiber, 50/50 beam splitter, and single-photon avalanche diode respectively.

2.2 EIT scheme

In this subsection we propose an EIT-based hyperentangled photon pair production scheme. This scheme is designed to produce photons that are entangled in the polarization and frequency degrees of freedom. In contrast to other schemes in the literature [6, 10], the entangled photon frequency states are separated by the ground state hyperfine splitting of ^{87}Rb. This results in frequency states that may be separated and recombined with low loss (for example, using a fiber Bragg grating), and that are directly compatible with storage in an EIT-based rubidium quantum memory.

The energy level diagram with relevant write/read fields and spontaneously emitted photons is shown in figure 4. Similar to the Raman scheme, initially all the atoms are optically pumped to the $|\mathrm{F}=1,\mathrm{m_F}=0\rangle$ state. A write beam, field E_1 in figure 4, resonant on $|\mathrm{F}=1,\mathrm{m_F}=0\rangle$ to $|\mathrm{F}'=1,\mathrm{m_{F'}}=0\rangle$ transition causes Raman scattering into $|\mathrm{F}=1,\mathrm{m_F}=\pm1\rangle$ or $|\mathrm{F}=2,\mathrm{m_F}=\pm1\rangle$. Followed by a read beam (retroreflected write beam) excitation which Raman scatter the atoms back to the original state. The read beam can be field E_1 or E_2 where the later is resonant on $|\mathrm{F}=2,\mathrm{m_F}=0\rangle$ to $|\mathrm{F}'=2,\mathrm{m_{F'}}=0\rangle$ transition. Note that $|\mathrm{F}=1,\mathrm{m_F}=0\rangle$ to $|\mathrm{F}'=1,\mathrm{m_{F'}}=0\rangle$ and $|\mathrm{F}=2,\mathrm{m_F}=0\rangle$ to $|\mathrm{F}'=2,\mathrm{m_{F'}}=0\rangle$ are not allowed due to selection rules, the scattering is therefore off-resonant from nearby levels. To infer the two-photon hyperentangled state, we can break down the scheme into two parts.

In the first part, write beam is the field E_1 and read beam is the field E_2. The two paths that can interfere are:

1 $|\mathrm{F}=1,\mathrm{m_F}=0\rangle \rightarrow |\mathrm{F}'=1,\mathrm{m_{F'}}=0\rangle \rightarrow |\mathrm{F}=2,\mathrm{m_F}=+1\rangle \rightarrow$
$|\mathrm{F}'=2,\mathrm{m_{F'}}=+1\rangle \rightarrow |\mathrm{F}=1,\mathrm{m_F}=0\rangle$

2 $|\mathrm{F}=1,\mathrm{m_F}=0\rangle \rightarrow |\mathrm{F}'=1,\mathrm{m_{F'}}=0\rangle \rightarrow |\mathrm{F}=2,\mathrm{m_F}=-1\rangle \rightarrow$
$|\mathrm{F}'=2,\mathrm{m_{F'}}=-1\rangle \rightarrow |\mathrm{F}=1,\mathrm{m_F}=0\rangle$

The spontaneously emitted two-photon state is of the form:

$$\Psi \propto \left(\alpha \left|\sigma^+\right\rangle_1 |\sigma^-\rangle_2 + \beta |\sigma^-\rangle_1 \left|\sigma^+\right\rangle_2\right) \bigotimes \gamma |\omega_1 - \Delta_{\mathrm{HF}}\rangle_1 |\omega_1 + \Delta\rangle_2 \tag{2}$$

where α, β, and γ are complex constants whereas ω_1, Δ_{HF}, and Δ are the frequency of field E_1 , hyperfine splitting between F=1 and F=0 and hyperfine splitting between F′=1 and F′=2 respectively.

In the second part, write and read beams are both the same field E_1. The two paths that can interfere are:

1 $|\mathrm{F}=1,\mathrm{m_F}=0\rangle \rightarrow |\mathrm{F}'=1,\mathrm{m_{F'}}=0\rangle \rightarrow |\mathrm{F}=1,\mathrm{m_F}=+1\rangle \rightarrow$
$|\mathrm{F}'=1,\mathrm{m_{F'}}=+1\rangle \rightarrow |\mathrm{F}=1,\mathrm{m_F}=0\rangle$

2 $|\mathrm{F}=1,\mathrm{m_F}=0\rangle \rightarrow |\mathrm{F}'=1,\mathrm{m_{F'}}=0\rangle \rightarrow |\mathrm{F}=1,\mathrm{m_F}=-1\rangle \rightarrow$
$|\mathrm{F}'=1,\mathrm{m_{F'}}=-1\rangle \rightarrow |\mathrm{F}=1,\mathrm{m_F}=0\rangle$

The spontaneously emitted two-photon state is of the form:

$$\Psi \propto \left(\alpha \left|\sigma^+\right\rangle_1 |\sigma^-\rangle_2 + \beta |\sigma^-\rangle_1 \left|\sigma^+\right\rangle_2\right) \bigotimes \gamma |\omega_1\rangle_1 |\omega_1\rangle_2 \tag{3}$$

Considering both the aforementioned parts, we can infer the total two-photon state to be of the form:

$$\Psi \propto \left(\alpha \left|\sigma^{+}\right\rangle_1 \left|\sigma^{-}\right\rangle_2 + \beta \left|\sigma^{-}\right\rangle_1 \left|\sigma^{+}\right\rangle_2\right) \bigotimes \left(\gamma \left|\omega_1\right\rangle_1 \left|\omega_1\right\rangle_2 + \chi \left|\omega_1 - \Delta_{\mathrm{HF}}\right\rangle_1 \left|\omega_1 + \Delta\right\rangle_2\right) \tag{4}$$

where α, β, γ, and χ are complex constants. We expect to measure a hyperentangled two-photon state of this form.

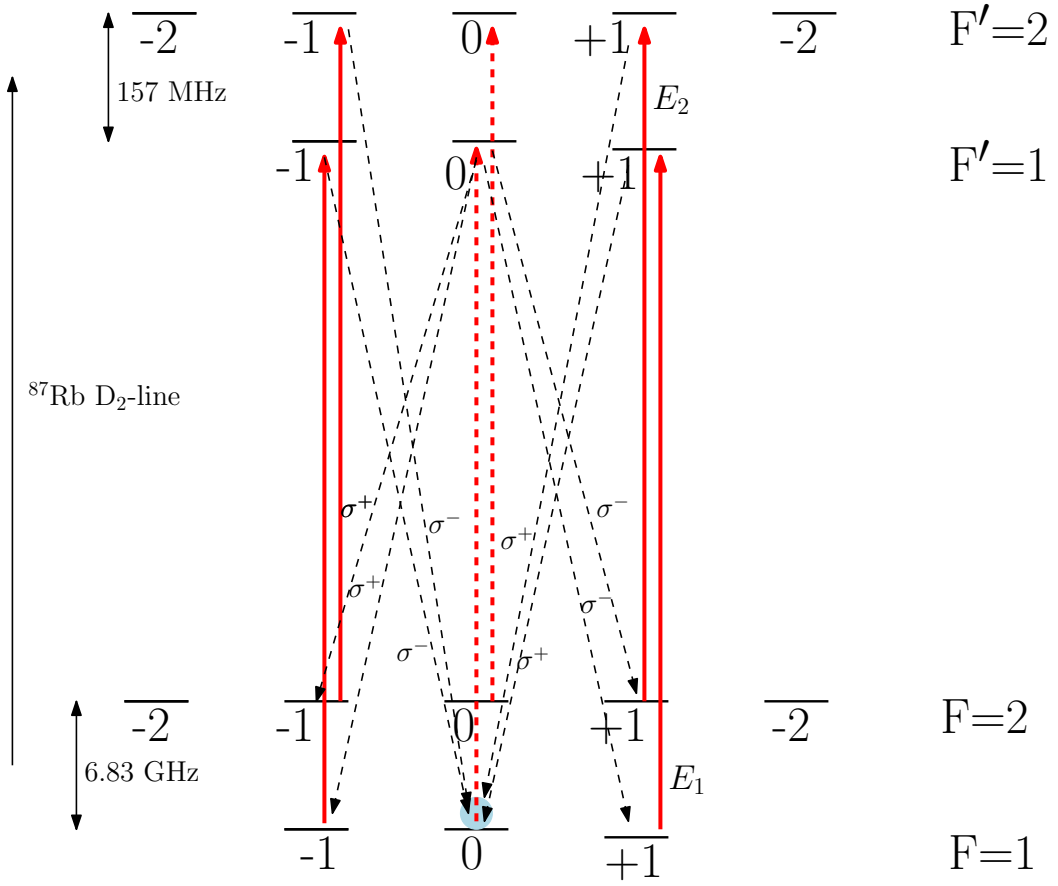

Fig. 4—Schematic of an EIT-based level scheme for hyperentangled photon pair production using ^{87}Rb D$_2$ line. Solid straight lines indicate absorption and dashed lines indicate spontaneous emission.

3. BEAM GEOMETRY

In this section we discuss geometry of the relevant beams and the bias magnetic field. As discussed in the section 2, we implement a right-angle geometry between write/read beams and Stokes/anti-Stokes emission axis. Real implementation of the schematic of figure 3 is shown in figure 5. Due to experimental constraints of the cooling beam propagating along the main MOT axis (z-direction), the bias field for optical pumping is applied at ~14 degrees to the z-axis. The linearly polarized optical pumping beam is adjusted to propagate along the bias field and is retroreflected. The write/read beam propagates along the y-direction and is retroreflected. The polarization of the write/read beam is set such that the electric field vector is aligned

along the bias field. Ideally the Stokes/anti-Stokes collection axis should be aligned along the bias field direction to minimize Rayleigh scattering; however, due to experimental constraints, the collection axis is at ~19 degrees to the z-axis.

Stokes and anti-Stokes fields are coupled into two single-mode fibers using standard aspheric lenses located ~23 cm from the atoms. The Gaussian beam waist diameter of each collection mode at the atoms is ~130 μm.

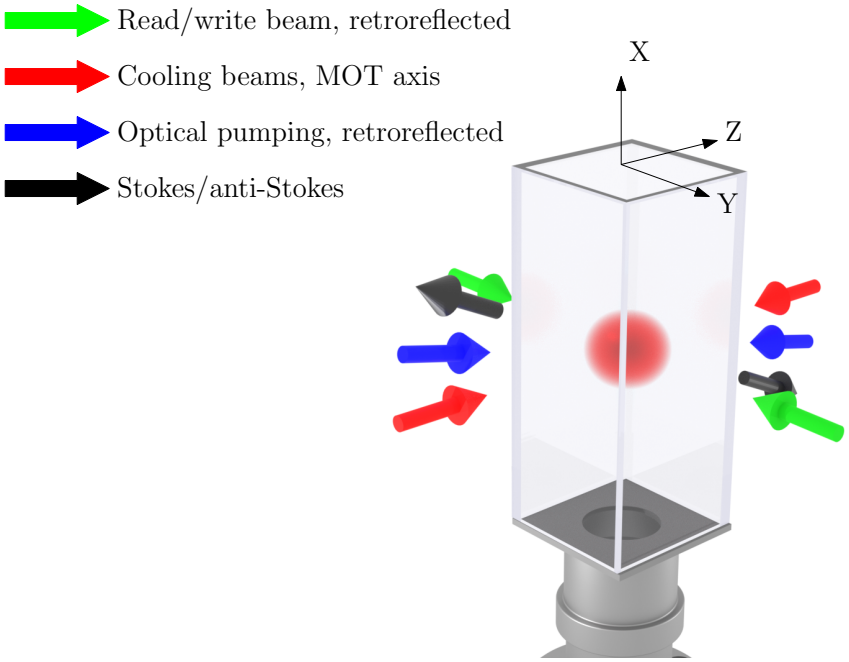

Fig. 5—Schematic of various laser beams with respect to the MOT.

4. COLD ATOM APPARATUS

The cold atom apparatus we use is a standard 3D MOT loaded from a 2D MOT. The glass-and-silicon vacuum cell, magnetic coils, and laser delivery optics are provided by a commercial system from ColdQuanta, with technical details similar to those described in reference [16]. The cooling laser is a Toptica 780 nm extended cavity diode laser locked to a rubidium saturated absorption spectroscopy cell and amplified by a tapered amplifier. Frequency control and switching are provided by a set of single-pass and double-pass acousto-optic modulators.

There are two key requirements for the nonclassical photon pair generation methods investigated in this program: high optical depth (OD) of the cold atomic cloud on the relevant atomic transition and optical pumping to a single Zeeman state. The former is necessary for enhancement of the nonlinear four-wave mixing mechanism responsible for photon correlations [14, 17] and the later is only specific to the level scheme in our experiment. A significant experimental challenge in this experiment is the simultaneous realization of both these conditions.

4.1 Optical depth

In our experiments we achieve high optical depth (OD) using two related methods. In the first method method we load the MOT at a quadrupole field gradient and cooling light detuing of ∼7.5 G/cm and ∼-9 MHz, respectively. Although the MOT loading rate is maximum under these parameters, the OD is only approximately 2. We increase the density and OD by carrying out a compressed MOT (CMOT) [18] step simply by further detuning the cooling light to ∼-60 MHz for ∼10 ms. In the second method, we load the 3D MOT at a higher quadrupole field gradient of $\gtrsim$11 G/cm and a higher cooling light detuning of $\gtrsim$-15 MHz. Under these parameters we capture a smaller total atom number while realizing a higher atomic density and a higher OD.

To accumulate photon statistics rapidly, experimental schemes optimizing duty cycle are often used. In this case, we employ the second method since it eliminates the CMOT stage and ∼10% atom loss during a CMOT stage while maintaining high enough optical depth. In our experiment, this method allows us to perform an initial long MOT loading followed by ∼100 experimental runs before observing ∼10% atom loss. An example of this experimental sequence is shown in figure 6.

An experimental scheme where the duty cycle is lowered due to inclusion of intermediate steps such as turning off trap beams, quadrupole field turn off, application of a bias field, and optical pumping leads to loss in optical depth due to free expansion of the gas during the interval. In such cases, having an initial CMOT stage prior to the intermediate steps leads to a sufficiently high optical depth even after the intermediate steps. This is necessary for implementation of our experimental scheme where the atoms are optically pumped to $|F = 1, m_F = 0\rangle$. An example of this experimental sequence is shown in figure 7.

Figures 8 and 9 are representative of typical optical depths in our experiment. The data was taken at a quadrupole field gradient of 11 G/cm and a cooling light detuning of -15 MHz during the MOT loading stage followed by an optical depth measurement. The two figures indicate enhancement in OD with a CMOT stage. The optical depth is measured using absorption imaging technique on the F=1 to F′=2 transition [19, 20].

4.2 Optical pumping

We use a single linearly polarized laser beam with two frequency components to optically pump atoms to $|F = 1, m_F = 0\rangle$ state. The laser beam propagates along the direction of a bias field (∼290 mG) as discussed in section 3. One frequency component is resonant on F=2 to F′=2 transition which depumps atoms from F=2 to F=1 ground hyperfine manifold while the other frequency component is resonant on F=1 to F′=0 transition. In the presence of the linearly polarized light resonant on F=1 to F′=0 transition, atoms are pumped to the dark-state $|F = 1, m_F = 0\rangle$. To quantitively verify optical pumping efficiency, we carry out microwave spectroscopy. Once atoms are optically pumped, we apply a microwave Π-pulse on the $|F = 1, m_F = 0\rangle$ to $|F = 2, m_F = 0\rangle$ clock transition followed by a pulse of cooling light on F=2 to F′=3 transition to determine the transfer. Due to technical limitation of the microwave apparatus, we can estimate that at least 80% of the atoms are transferred to the $|F = 1, m_F = 0\rangle$ state. Typical populations in $m_F = -1$, $m_F = 0$, and $m_F = +1$ after optical pumping are shown in figures 10, 11, and 12 respectively.

Optical pumping beam is ∼5 mm in diameter with ∼0.5 mW power and a typical pumping duration is ∼1 ms. Relative power between the two frequency components are set by adjusting the drive power to an EOM in the optical pumping beam path. The drive power is set for optimum optical pumping to the $|F = 1, m_F = 0\rangle$ state.

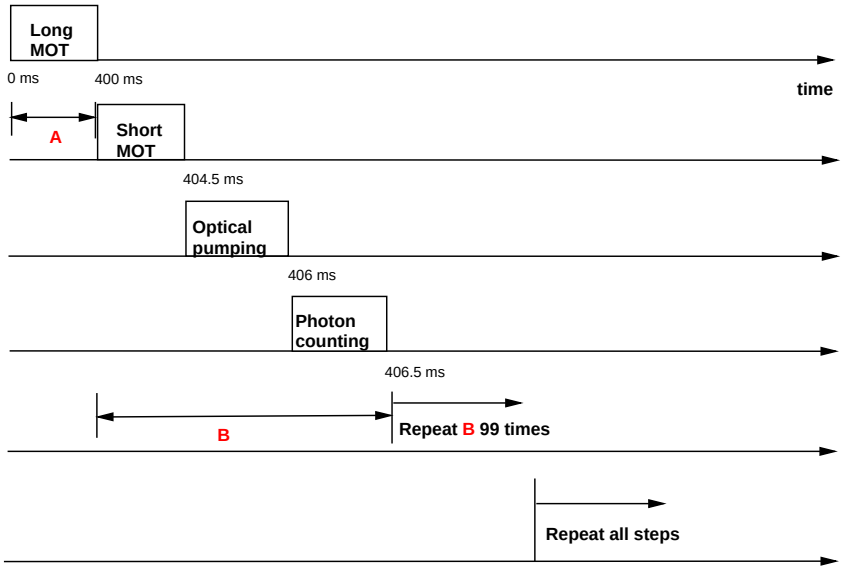

Fig. 6—Example of a high duty cycle experimental sequence.

We find that an unintended consequence of high optical depth along the pump direction is poor optical pumping. As shown by data in figures 10, 11, and 12 with a CMOT in the experimental sequence which leads to a higher optical depth, we find poorer depletion of the $|F = 1, m_F = \pm 1\rangle$ states. We speculate that residual populations in the $m_F = \pm 1$ states may degrade the observation of the intended four-wave-mixing process.

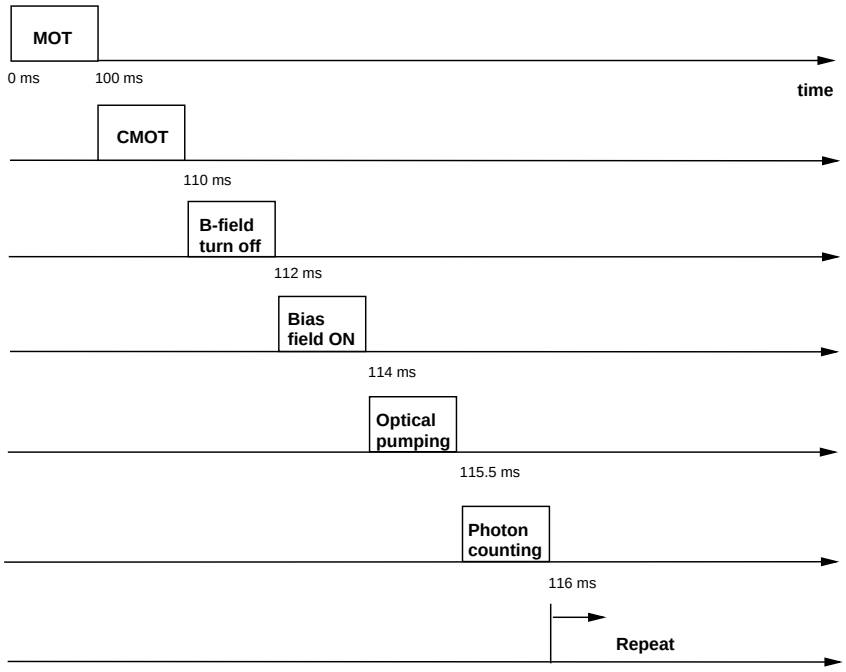

Fig. 7—Example of a low duty cycle experimental sequence.

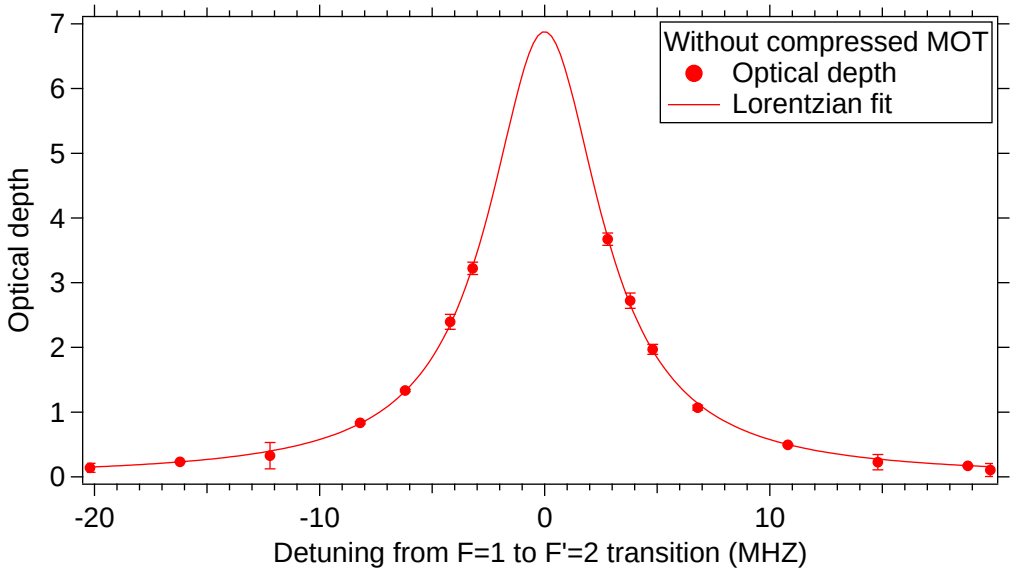

Fig. 8—Optical depth as a function of detuning without an initial CMOT stage in the experimental sequence.

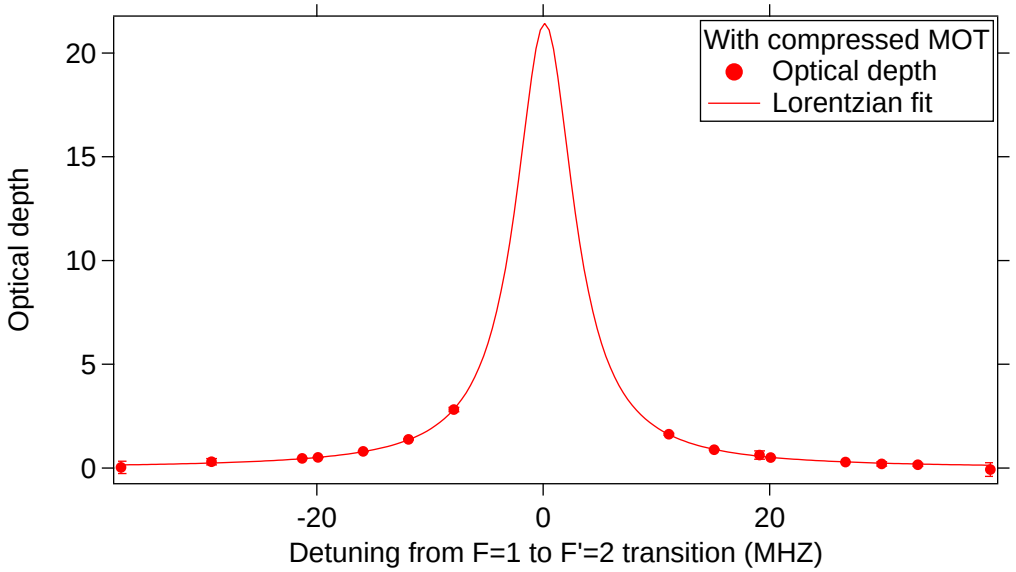

Fig. 9—Optical depth as a function of detuning with an initial CMOT stage in the experimental sequence.

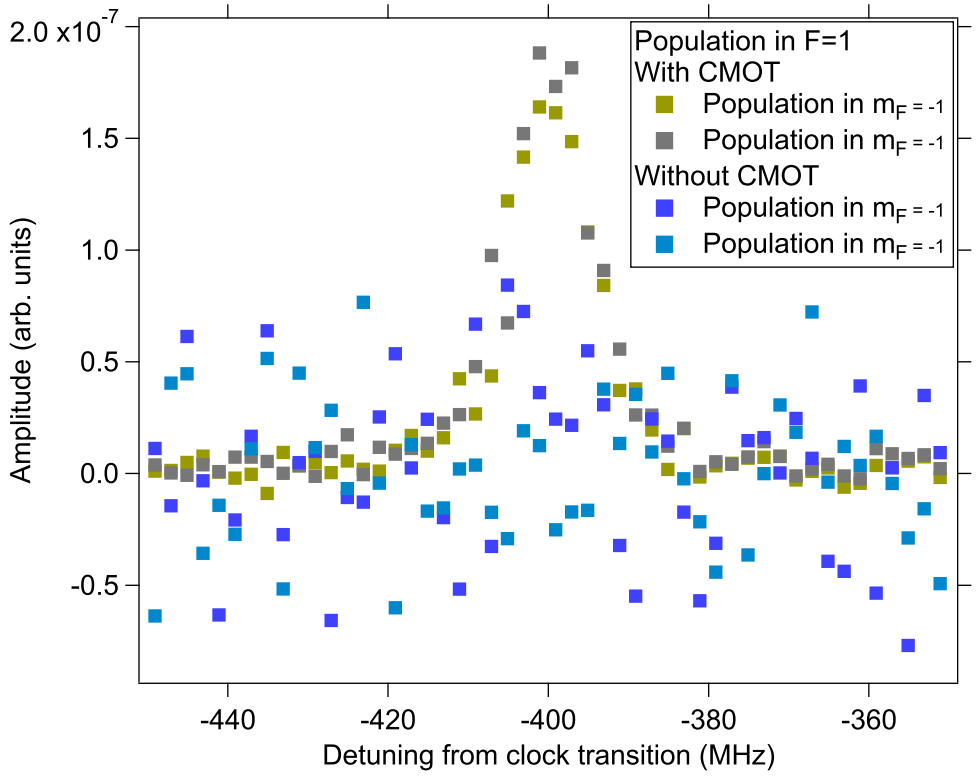

Fig. 10—Fluorescence measurement of atomic population in $|F = 1, m_F = -1\rangle$ after optical pumping. Populations are shown with and without a CMOT stage.

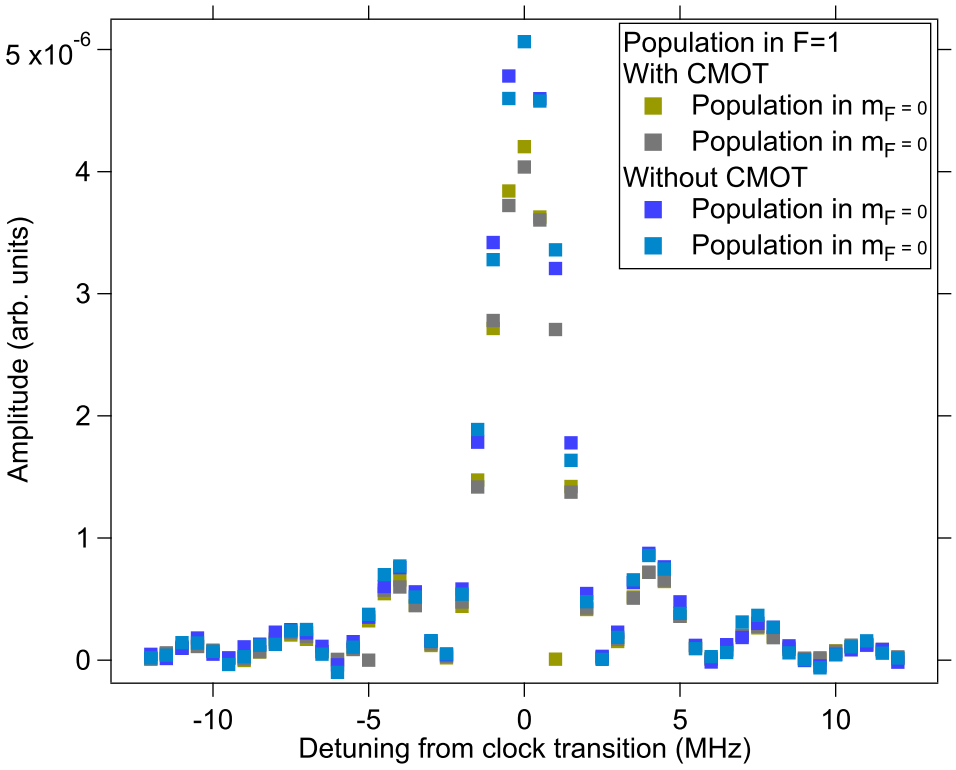

Fig. 11—Fluorescence measurement of atomic population in $|F = 1, m_F = 0\rangle$ after optical pumping. Populations are shown with and without a CMOT stage.

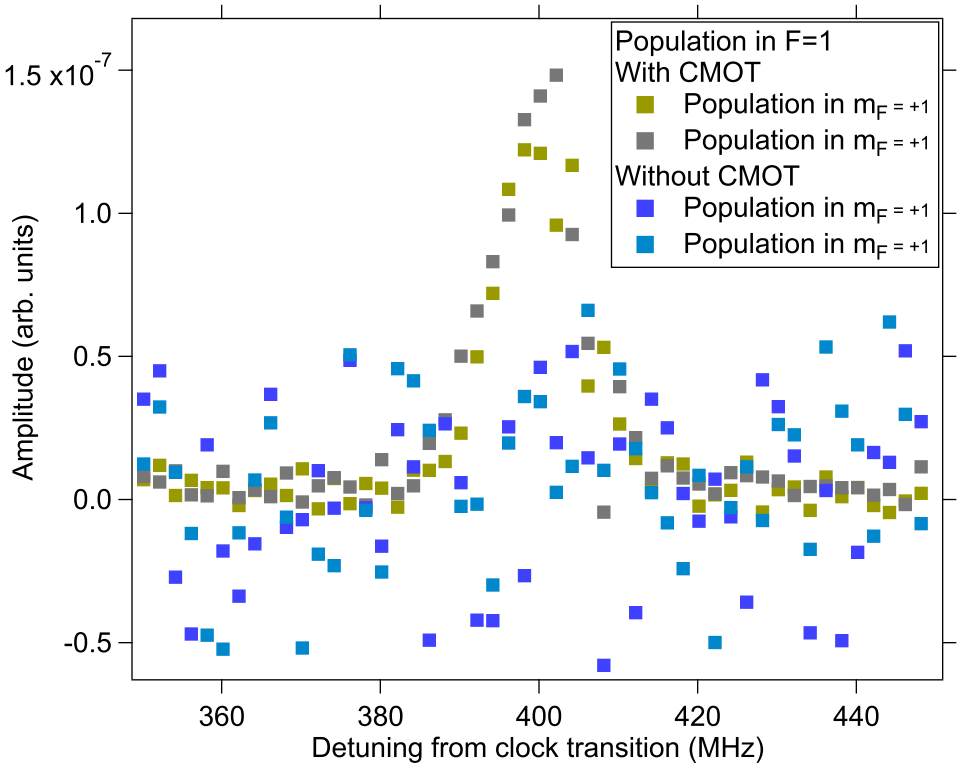

Fig. 12—Population in $|F = 1, m_F = +1\rangle$ after optical pumping. Populations are shown with and without a CMOT stage.

5. MEASUREMENTS

Entangled photons are non-classically correlated [21]. A first step in verifying entanglement is to measure non-classical intensity correlations between photons and establish whether the measured correlations violate Cauchy-Schwartz inequality [9, 21]. We measure cross-correlations between Stokes and anti-Stokes fields and respective auto-correlations followed by evaluation of the inequality:

$$(g_{12}^{(2)}(\tau))^2 \leq g_{11}^{(2)}(0) g_{22}^{(2)}(0) \tag{5}$$

where $g_{12}^{(2)}$ is the normalized cross-correlation and $g_{22}^{(2)}, g_{11}^{(2)}$ are normalized auto-correlations. Standard photon counting techniques are used to measure these quantities [22, 23]. The photon counting measurements are done after all the preparatory steps as indicated in figures 6 and 7. Stokes and anti-Stokes photon counting is carried out simultaneously while the write/read laser beam is incident on the cold atom cloud. Experiments are carried out at laser detunings and intensities at which non-classical correlations were observed in prior experiments with similar cold atoms parameters [9, 14].

Additionally, we have explored the influence of the atom cloud geometry on the four-wave-mixing process. Rather than directly alter the distribution of atomic positions, we have instead modified the pump laser beam geometry. For a large, circular pump beam, the entire atom cloud contributes to the four-wave-mixing process. On the other hand, for a highly elliptical pump beam, the participating atom cloud is optically thin in the direction perpendicular to the detection axis while having high optical depth along the detection axis. In either case, only those emitted photons within the effective aperture of the detection fiber are measured. The following two cases were studied:

1. Circular beam of ~4.3 mm diameter.
2. Elliptical beam with ~4.4 mm x 0.062 mm diameter.

A ^{87}Rb level diagram with relevant detuning and write/read beam profile with respect to the Stokes/anti-Stokes axis is shown in figure 13.

5.1 Raman scheme

In this subsection we discuss experimental measurements relevant to the Raman scheme discussed in section 2.1. The experiments were conducted in two steps. First we implement the Raman scheme with atoms optically pumped to F=1 state but not necessarily to the single Zeeman state $m_F = 0$. Second we move to the full Raman scheme where we start with all the atoms optically pumped to $|F = 1, m_F = 0\rangle$.

We begin by implementing a system in which observation of nonclassically correlated photon pairs is expected based on prior work. In this initial scheme, the single retroreflected pump beam is configured to provide an off-resonant write beam and on-resonance read beam (figure 13). In this configuration, similar to the experiment carried out by Kolchin et al. [14], nonclassically correlated photon pairs are clearly observed through the violation of the Cauchy-Schwartz inequality. Next we change the detuning and appropriately adjust write/read beam intensity and again measure the photon correlations. A sample of key results with a

circular pump beam is shown in figure 14 and with an elliptical pump beam is shown in figures 15 and 16. These data are taken with atoms optically pumped to the ground F=1 hyperfine level but not necessarily to the single Zeeman $m_F = 0$. All the lasers apart from the pump are extinguished and the quadrupole field of the MOT is left on during the photon couting interval for the data shown in this section. The normalized auto-correlations, $g_{11}^{(2)}(0)$ and $g_{22}^{(2)}(0)$ are ~1.2 for the data and are not shown in the figures.

The data for the initial on-resonance case shown in figure 14 was taken under similar conditions as the experiment described by Kolchin et al [14]. We observe damped oscillations in the cross-correlation function whose period is close to $1/\sqrt{\Omega_c^2 + \delta^2}$ where Ω_c and δ are the coupling field Rabi frequency on F=2 to F′=2 transition and detuning from the transition, respectively. For the on-resonance case where $\delta = 0$, a coupling beam with ~2.15 mm waist and ~210 mW power we obtain a RMS Rabi frequency of ~72 MHz and a Rabi period of ~13.2 ns. This value is fairly close to the Rabi period of ~9 ns observed in the data. The RMS Rabi frequency is defined as $\sqrt{\frac{1}{5}\sum_{i=1}^{5}\Omega_i^2}$ where Ω_i is the Rabi frequency from $|F = 2, m_F\rangle$ to $|F' = 2, m_F\rangle$. We point out that, as discussed by Kolchin et al. [14], the cross-correlation behaves differently based on the experimental parameters such as coupling Rabi frequency, optical depth, and decoherence of the ground state coherence between F=1 and F=2 during the EIT process. Our work did not extensively explore the experimental parameter space of the on-resonance case.

Next we investigate photon correlations as we depart from the on-resonance scheme. When the read beam is detuned to the red by 0.5 GHz from the $5P_{3/2}$, we observe diminished non-classical correlations. The cross-correlation in this case show higher-frequency oscillatory structure, which we speculate may be due to the fact that the off-resonant read beam is now interacting with multiple hyperfine states of the $5P_{3/2}$ level. Interestingly, when the read beam is instead blue-detuned by an equal amount, we observe only classical correlations. This strong asymmetry between red and blue detunings in atomic four-wave-mixing is surprising and has not, to our knowledge, been previously observed. Similar observations are made in the case of an elliptical write/read beam as shown in figure 15. Additionally, for the elliptical write/read beam case we carried out identical set of measurements where we pump most of the atoms to $|F = 1, m_F = 0\rangle$ state and observe same behaviour with respect to detuning (data not shown in this report).

As read beam detuning is further increased, cross-correlations diminish as shown in figure 16 despite an increase in pump beam intensity to maintain similar scattering rates into the Stokes/anti-Stokes collection modes. Asymmetry in the cross-correlation between red vs blue detuing is observable even at 1.5 GHz detuning. We note that our observation window for cross-correlation is typically [-250 ns, 250 ns] or larger and only the relevant portion of the cross-correlation functions are shown.

In summary, experiments conducted using the Raman scheme indicate that, under the experimental parameters explored, the Stokes/anti-Stokes photons are only classically correlated in the Raman scheme where the write/read laser is detuned by half the ground-state hyperfine splitting of ^{87}Rb . A gradual falloff in correlation is observed as the pump is tuned away from resonance on the red side, while a more sudden elimination of correlations is observed on the blue side of resonance. The origin of this asymmetry remains under investigation.

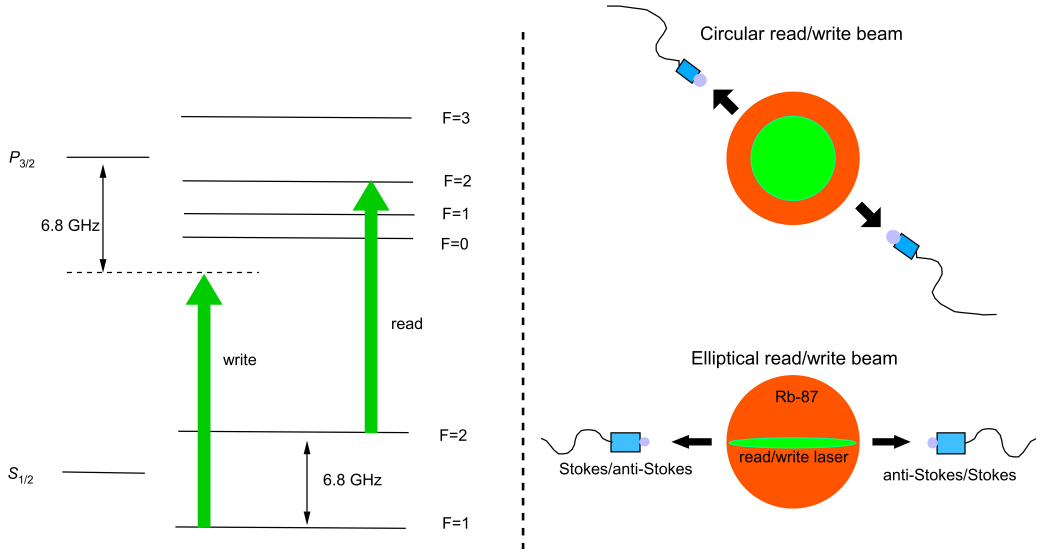

Fig. 13—Simplified level structure with relevant read/write laser frequencies on the left. Schematic of the read/write beam geometries implemented.

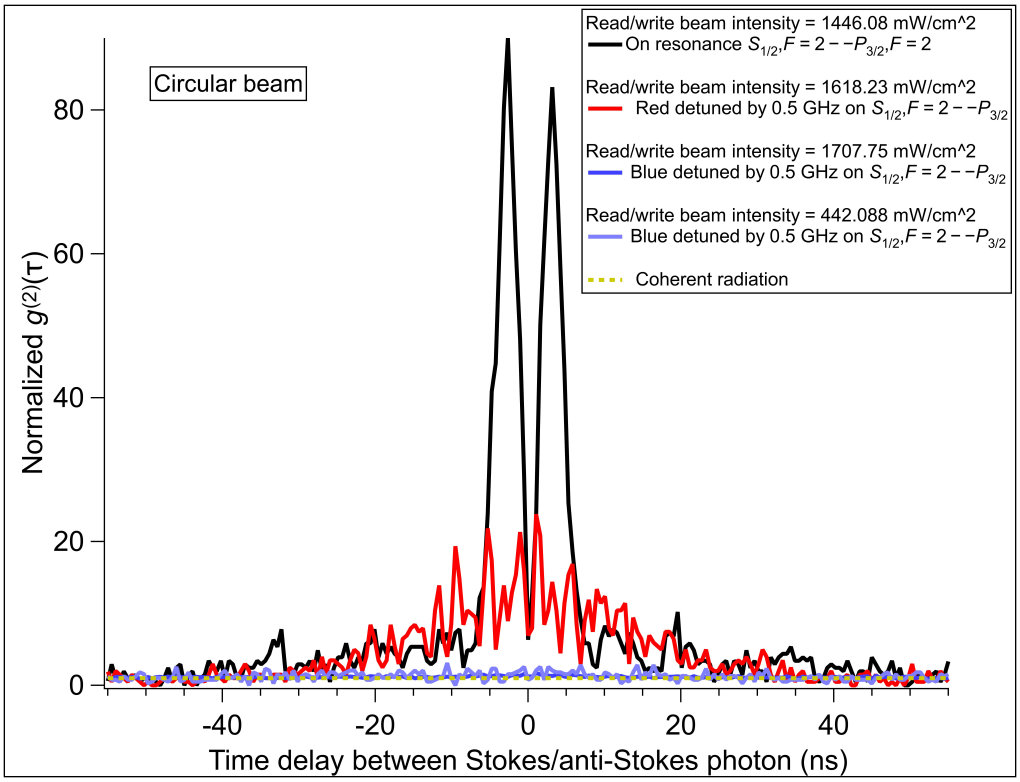

Fig. 14—Normalized $g_{12}^{(2)}(\tau)$ for different detunings. The read/write beam is circular as described in the text. Histogram bin width used is 0.53 ns. Adjacent points are connected using lines in the figure.

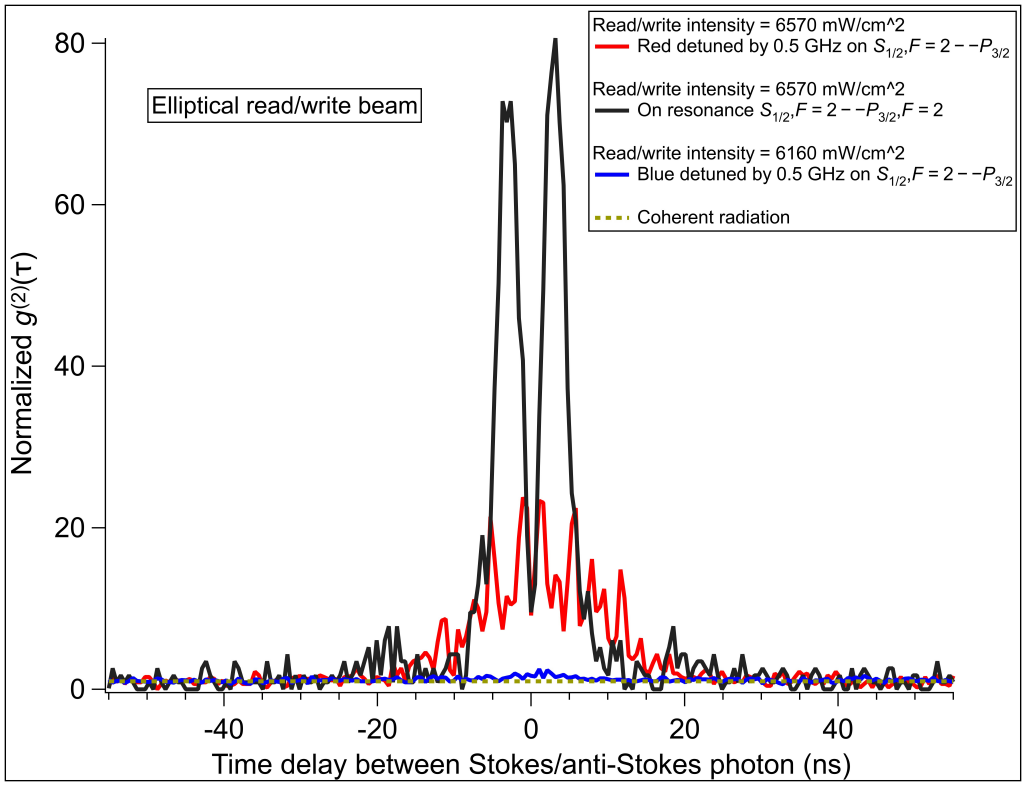

Fig. 15—Normalized $g_{12}^{(2)}(\tau)$ for different detunings. The read/write beam is elliptical as described in the text. Histogram bin width used is 0.53 ns. Adjacent points are connected using lines in the figure.

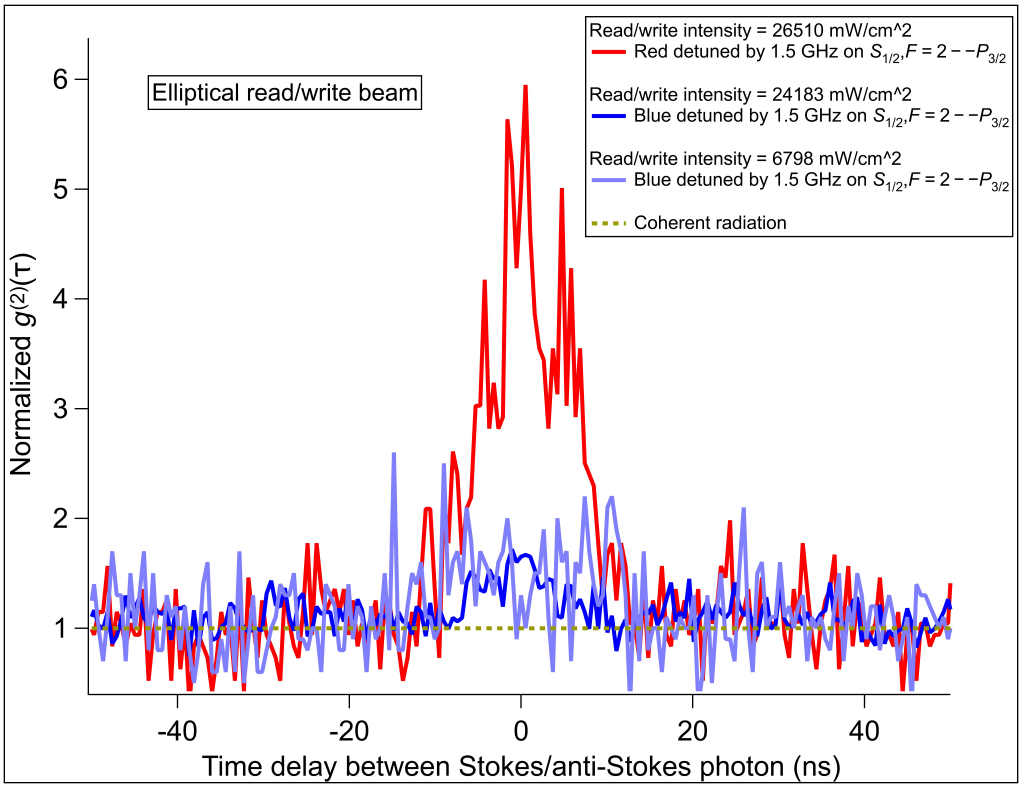

Fig. 16—Normalized $g_{12}^{(2)}(\tau)$ for different detunings. The read/write beam is elliptical as described in the text. Histogram bin width used is 0.53 ns. Adjacent points are connected using lines in the figure.

5.2 EIT scheme

In this subsection we describe our investigation into the EIT-based scheme proposed in section 2.2. We developed this new scheme following the observation in the previous section that nonclassical photon correlations are eliminated when the "read" field is far from resonance. This scheme is designed to provide multiple, simultaneous four-wave-mixing paths while maintining the resonance condition for the read field. Implementation of the scheme is carried out as follows:

1. Optically pump most of the atoms into $|\mathrm{F} = 1, \mathrm{m_F} = 0\rangle$ ground state.
2. Turn on the pump beam with field E_1 and E_2 (figure 4) simultaneously. Relative strength between the fields is controlled by RF drive power to an EOM in the beam path. Carrier field is E_2 and E_1 is a sideband. The carrier field power is low enough that there is negligible off-resonance scattering from atoms in F=1.
3. Carry out cross-correlation measurements as a function of various E_1 powers.

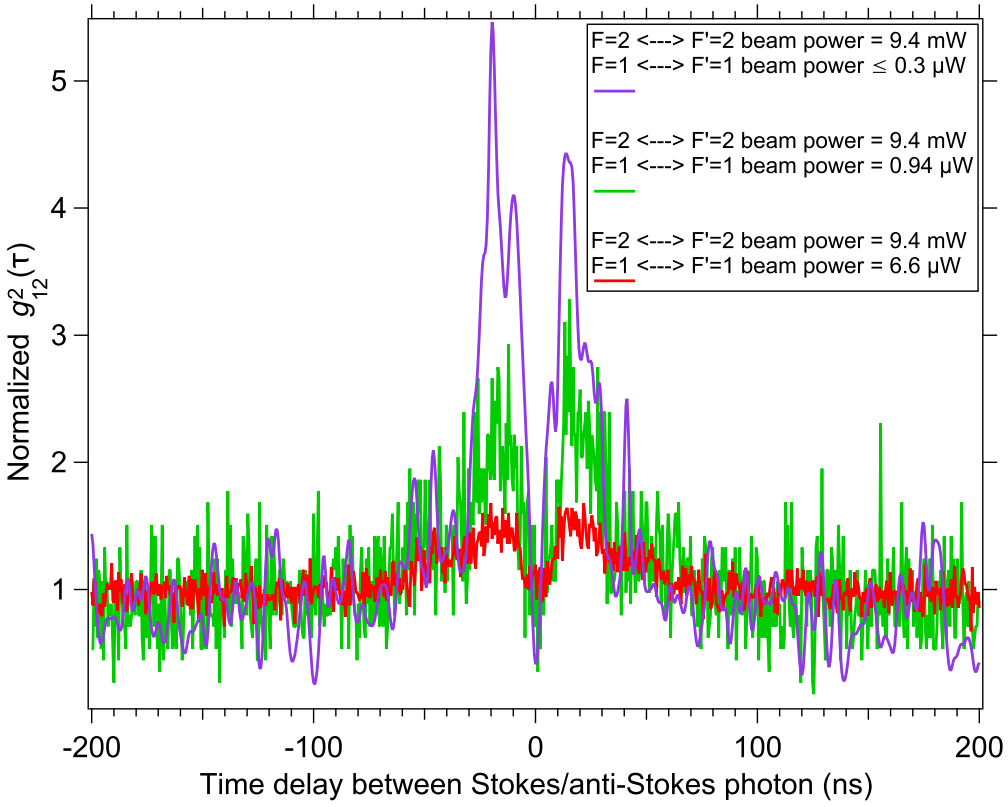

Fig. 17—Normalized $g^{(2)}_{12}(\tau)$ for different drive powers on the F=1 to F'=1 transition. The read/write beam is circular as described in the text. Histogram bin width used is 0.53 ns. Adjacent points are connected using lines in the figure.

Preliminary results are shown in figure 17. The normalized auto-correlations, $g^{(2)}_{11}(0)$ and $g^{(2)}_{22}(0)$ are ~1.2 for the data and are not shown in the figures. The write/read beam is circular and has a diameter ~4.3

mm and a bias field of ∼290 mG is used to define quantization axis for optical pumping. Only the bias field and the write/read beam are on during the photon counting interval. The powers of the fields E_1 and E_2 are indicated in the figure.

We make the following observations:

1. We find a qualitatively similar cross-correlation shape similar to the resonant case shown in figure 14 and discussed in section 5.1. There are two different read fields, E_1 and E_2, with powers ratio > 1/1000.

2. The cross-correlations are highly diminished and decrease further as we increase the power of field E_1. This is unexpected.

3. Experimentally, E_2 is the dominant read field and we expect it to dominate the cross-correlation. Similar to the analysis done in 5.1, using the E_2 field power of 9.4 mW and the beam waist of 2.15 mm, the peak Rabi frequency for the $|\mathrm{F} = 2, \mathrm{m_F} = 1\rangle$ to $|\mathrm{F}' = 2, \mathrm{m_{F'}} = 1\rangle$ transition is ∼11 MHz. This translates to a Rabi period of ∼92 ns which is within a factor of 2 of the observed damping period of the ∼50 ns observed in the data.

4. Fields E_1 and E_2 are responsible for two four-wave mixing processes that are enhanced due to EIT. The level scheme shown in figure 4 requires that transparency be established for multiple emitted fields in order for EIT to be effective. In such a case, there may be interference effects that reduce the efficacy of EIT and give rise to diminished cross-correlations.

6. CONCLUSIONS

We have studied the production of nonclassically correlated photon pairs from a laser-cooled rubidium ensemble in a variety of pump configurations that may be expected to lead to the production of polarization-frequency hyperentangled states. Interestingly, nonclassical correlations are either strongly diminished or entirely eliminated in schemes that were expected to optimally produce photons entangled in frequency using the ground-state hyperfine splitting. It is likely that the interference between multiple four-wave-mixing, absorption, and EIT processes leads to this reduction of correlations.

A number of other unexpected results were observed. After reproducing the generation of photon pairs using the scheme of Ref. [14], we attempted to operate the four-wave-mixing process away from resonance. We found that moving the pump laser frequencies below resonance retained nonclassical correlations at a reduced level, while moving them above resonance entirely eliminated observable correlations. We have speculated that possible reasons for this detuning asymmetry may include mechanical effects on the atoms due to the optical potential of the pump beam, absorption by nearby transitions, or else a disruption of phase matching due to dispersion. Additionally, we observed that the addition of a small (< 0.1%) sideband driving the $|F = 1\rangle \rightarrow |F' = 1\rangle$ transition is sufficient to virtually eliminate nonclassical photon correlations in a four-wave-mixing system similar to [14].

This project involved a number of refinements to the cold-rubidium experiment. These included the optimization of optical depth using a compressed MOT, the characterization and optimization of optical pumping using microwave spectroscopy, and the optimization of duty cycle required to obtain the necessary

photon counting statistics. The apparatus is well-situated for future quantum entanglement, quantum memory, or quantum optics experiments.

REFERENCES

1. N. Gisin and R. Thew, "Quantum communication," *Nature Photonics* **1**, 165–171 (3 2007), ISSN 17494885, doi:10.1038/nphoton.2007.22.
2. H. J. Kimble, "The quantum internet," 6 2008, ISSN 14764687.
3. J. T. Barreiro, N. K. Langford, N. A. Peters, and P. G. Kwiat, "Generation of hyperentangled photon pairs," *Physical Review Letters* **95**, 260501 (12 2005), ISSN 00319007, doi:10.1103/PhysRevLett.95.260501.
4. M. Prilmüller, T. Huber, M. Müller, P. Michler, G. Weihs, and A. Predojević, "Hyperentanglement of Photons Emitted by a Quantum Dot," *Physical Review Letters* **121**, 110503 (9 2018), ISSN 10797114, doi:10.1103/PhysRevLett.121.110503.
5. M. X. Dong, W. Zhang, S. Shi, K. Wang, Z. Y. Zhou, S. L. Liu, D. S. Ding, and B. S. Shi, "Two-color hyper-entangled photon pairs generation in a cold ^{85}Rb atomic ensemble," *Optics Express* **25**, 10145 (5 2017), ISSN 1094-4087, doi:10.1364/oe.25.010145.
6. T. M. Zhao, Y. S. Ihn, and Y. H. Kim, "Direct Generation of Narrow-band Hyperentangled Photons," *Physical Review Letters* **122**, 123607 (3 2019), ISSN 0031-9007, doi:10.1103/PhysRevLett.122.123607.
7. M. Halder, A. Beveratos, R. T. Thew, C. Jorel, H. Zbinden, and N. Gisin, "High coherence photon pair source for quantum communication," *New Journal of Physics* **10**, 23027 (2 2008), doi:10.1088/1367-2630/10/2/023027. URL `https://doi.org/10.1088%2F1367-2630%2F10%2F2%2F023027`.
8. A. Kuzmich, W. P. Bowen, A. D. Boozer, A. Boca, C. W. Chou, L. M. Duan, and H. J. Kimble, "Generation of nonclassical photon pairs for scalable quantum communication with atomic ensembles," 6 2003, ISSN 00280836.
9. V. Balić, D. A. Braje, P. Kolchin, G. Y. Yin, and S. E. Harris, "Generation of Paired Photons with Controllable Waveforms," *Physical Review Letters* **94**, 183601 (5 2005), ISSN 0031-9007, doi:10.1103/PhysRevLett.94.183601.
10. H. Yan, S. Zhang, J. F. Chen, M. M. T. Loy, G. K. L. Wong, and S. Du, "Generation of Narrow-Band Hyperentangled Nondegenerate Paired Photons," *Physical Review Letters* **106**, 033601 (1 2011), ISSN 0031-9007, doi:10.1103/PhysRevLett.106.033601.
11. M. D. Lukin, P. R. Hemmer, M. Löffler, and M. O. Scully, "Resonant Enhancement of Parametric Processes via Radiative Interference and Induced Coherence," *Physical Review Letters* **81**, 2675–2678 (9 1998), ISSN 0031-9007, doi:10.1103/PhysRevLett.81.2675.
12. M. D. Lukin, A. B. Matsko, M. Fleischhauer, and M. O. Scully, "Quantum Noise and Correlations in Resonantly Enhanced Wave Mixing Based on Atomic Coherence," *Physical Review Letters* **82**, 1847–1850 (3 1999), ISSN 0031-9007, doi:10.1103/PhysRevLett.82.1847.
13. S. E. Harris, J. E. Field, and A. Imamo(U) glu, "Nonlinear optical processes using electromagnetically induced transparency," *Physical Review Letters* **64**, 1107–1110 (3 1990), ISSN 0031-9007, doi:10.1103/PhysRevLett.64.1107.

14. P. Kolchin, S. Du, C. Belthangady, G. Y. Yin, and S. E. Harris, "Generation of Narrow-Bandwidth Paired Photons: Use of a Single Driving Laser," *Physical Review Letters* **97**, 113602 (9 2006), ISSN 0031-9007, doi:10.1103/PhysRevLett.97.113602.

15. A. Aspect, P. Grangier, and G. Roger, "Experimental Tests of Realistic Local Theories via Bell's Theorem," *Physical Review Letters* **47**, 460–463 (8 1981), ISSN 0031-9007, doi:10.1103/PhysRevLett.47.460.

16. E. A. Salim, *Ultracold matter systems and atomtronics instrumentation.*, PhD thesis (University of Colorado at Boulder, 2011).

17. A. V. Gorshkov, A. André, M. Fleischhauer, A. S. Sørensen, and M. D. Lukin, "Universal Approach to Optimal Photon Storage in Atomic Media," *Phys. Rev. Lett.* **98**, 123601 (Mar 2007), doi:10.1103/PhysRevLett.98.123601. URL https://link.aps.org/doi/10.1103/PhysRevLett.98.123601.

18. W. Petrich, M. H. Anderson, J. R. Ensher, and E. A. Cornell, "Behavior of atoms in a compressed magneto-optical trap," *Journal of the Optical Society of America B* **11**, 1332 (8 1994), ISSN 0740-3224, doi:10.1364/JOSAB.11.001332.

19. W. Ketterle, D. S. Durfee, and D. M. Stamper-Kurn, "Making, probing and understanding Bose-Einstein condensates," 1999.

20. H. J. Lewandowski, D. M. Harber, D. L. Whitaker, and E. A. Cornell, "Simplified System for Creating a Bose–Einstein Condensate," *Journal of Low Temperature Physics* **132**, 309–367 (2003), ISSN 00222291, doi:10.1023/A:1024800600621.

21. L. Mandel and E. Wolf, *Optical Coherence and Quantum Optics* (Cambridge University Press, 1995), doi:10.1017/CBO9781139644105.

22. R. Brouri, A. Beveratos, J. P. Poizat, and P. Grangier, "Photon antibunching in the fluorescence of individual color centers in diamond," *Opt. Lett.* **25**(17), 1294–1296 (Sep 2000), doi:10.1364/OL.25.001294. URL https://opg.optica.org/ol/abstract.cfm?URI=ol-25-17-1294.

23. J. J. Thorn, M. S. Neel, V. W. Donato, G. S. Bergreen, R. E. Davies, and M. Beck, "Observing the quantum behavior of light in an undergraduate laboratory," *American Journal of Physics* **72**, 1210–1219 (9 2004), ISSN 0002-9505, doi:10.1119/1.1737397. URL /aapt/ajp/article/72/9/1210/532598/Observing-the-quantum-behavior-of-light-in-an.